ACCELERATION AND SUBSTRUCTURE CONSTRAINTS IN A QUASAR OUTFLOW

Patrick B. Hall,[1] Sarah I. Sadavoy,[1] Damien Hutsemekers,[2] John E. Everett,[3] Alireza Rafiee[1]

ABSTRACT

We present observations of probable line-of-sight acceleration of a broad absorption trough of C IV in the quasar SDSS J024221.87+004912.6. We also discuss how the velocity overlap of two other outflowing systems in the same object constrains the properties of the outflows. The Si IV doublet in each system has one unblended transition and one transition which overlaps with absorption from the other system. The residual flux in the overlapping trough is well fit by the product of the residual fluxes in the unblended troughs. For these optically thick systems to yield such a result, at least one of them must consist of individual subunits rather than being a single structure with velocity-dependent coverage of the source. If these subunits are identical, opaque, spherical clouds, we estimate the cloud radius to be $r \simeq 3.9 \times 10^{15}$ cm. If they are identical, opaque, linear filaments, we estimate their width to be $w \simeq 6.5 \times 10^{14}$ cm. These subunits are observed to cover the Mg II broad emission line region of the quasar, at which distance from the black hole the above filament width is equal to the predicted scale height of the outer atmosphere of a thin accretion disk. Insofar as that scale height is a natural size scale for structures originating in an accretion disk, these observations are evidence that the accretion disk can be a source of quasar absorption systems. Based on data from ESO program 075.B-0190(A).

Subject headings: quasars: general, absorption lines, individual (SDSS J024221.87+004912.6)

1. INTRODUCTION

Absorption systems in active galactic nuclei (AGN) can be classified as *intrinsic*, which are associated with the active nucleus and often outflowing from it, and *intervening*, which originate from clouds external to the AGN's environment. Determining an absorption system's classification can be difficult. A reliable indication of intrinsic absorption is time variability, such as a shift in the velocity of a given feature or changes in its absorption strength as a function of velocity. In the broad absorption line (BAL) troughs $\gtrsim 1000 \, \mathrm{km \, s^{-1}}$ wide which are most often found in the luminous AGN known as quasars, reports of time variable absorption strengths have been relatively common (Bromage et al. 1985; Foltz et al. 1987; Voit, Shull, & Begelman 1987; Smith & Penston 1988; Turnshek et al. 1988; Barlow, Junkkarinen, & Burbidge 1989, 1992a; Barlow et al. 1992b; Barlow 1994; Hamann et al. 1995; Michalitsianos, Oliversen, & Nichols 1996; Hamann, Barlow, & Junkkarinen 1997b; Barlow, Hamann, & Sargent 1997; Hamann et al. 1997a; Hall et al. 2002; Gallagher et al. 2004; Misawa et al. 2005; Lundgren et al. 2006). Such variability can even include the appearance or disappearance of absorption systems (Koratkar et al. 1996; Ganguly, Charlton, & Eracleous 2001; Ma 2002; Gallagher et al. 2005; Leighly et al. 2005). In contrast, velocity shifts in BAL outflows have been reported in only Q 1303+308 (Vilkoviskij & Irwin 2001) and Mrk 231 (Rupke, Veilleux, & Sanders 2002, and references therein), although Gabel et al. (2003)

have observed deceleration of a narrow absorber in the Seyfert 1 NGC 3783.

Acceleration must occur for AGN outflows to reach their observed velocities. Nonetheless, velocity shifts in AGN outflows are seen quite rarely because acceleration of an AGN outflow does not automatically translate into a change in its observed velocity profile, and vice versa. For example, a fixed mass loss rate into an outflow with a time-invariant driving force would yield a time-invariant acceleration profile with distance in the outflow, and thus produce unchanging absorption troughs. Arav et al. (1999) illustrate how radial acceleration of gas crossing our line of sight with a non-negligible transverse velocity produces an observed absorption trough with a broadened radial velocity profile that does not change with time. Since our lines of sight to AGN are essentially radial, and since AGN are fed by accretion disks consisting of gas with predominantly orbital velocities, most AGN outflows are expected to have non-negligible transverse as well as radial velocities. Thus, most intrinsic absorbers likely *are* exhibiting acceleration, disguised as a trough broader than the thermal or turbulent velocity width of the gas.

What are we then to make of cases where an outflow *does* exhibit a velocity shift? First, note that when our line of sight intersects the origin of an outflow, the absorption trough can start at zero line-of-sight velocity in the AGN rest frame, at least for ions present at the origin of the outflow. Ions present only downstream in an outflow, or lines of sight intersecting an outflow only downstream from its origin due to curvature in the flow lines, will produce 'detached' absorption troughs which do not start at zero velocity, as will a shell of material ejected in an intermittent outflow. With that in mind, consider possible explanations for a velocity shift observed in a detached absorption trough. Such a shift can be produced by changes in the ionization state as a function of

[1] Department of Physics and Astronomy, York University, 4700 Keele St., Toronto, Ontario M3J 1P3, Canada
[2] Senior Research Associate FNRS, University of Liège, Allée du 6 août 17, Bat. 5c, 4000 Liège, Belgium
[3] Departments of Physics and Astronomy and Center for Magnetic Self-Organization in Laboratory and Astrophysical Plasmas, University of Wisconsin-Madison, 1150 University Avenue, Madison, Wisconsin 53706, USA

velocity in a fixed outflow, by changes in the acceleration profile or geometry (or both) of such an outflow due to changes in the driving force or mass loss rate, or by actual line-of-sight acceleration of a shell of material from an intermittent outflow. Observations of velocity shifts are therefore worthwhile because they may yield insights into specific scenarios for quasar absorbers.

Here we present multiple-epoch observations (§2) of a quasar in which a broad absorption line trough of C IV increased in outflow velocity over 1.4 rest-frame years (§3). We also discuss how two overlapping outflows in the same quasar provide constraints on the properties of those outflows (§4). We end with our conclusions in §5.

2. OBSERVATIONS

The Sloan Digital Sky Survey (SDSS; York et al. 2000) is using a drift-scanning camera (Gunn et al. 1998) on a 2.5-m telescope (Gunn et al. 2006) to image $10^4 \deg^2$ of sky on the SDSS $ugriz$ AB magnitude system (Fukugita et al. 1996; Hogg et al. 2001; Smith et al. 2002; Pier et al. 2003; Ivezić et al. 2004). Two multi-fiber, double spectrographs are being used to obtain resolution $R \sim 1850$ spectra covering $\simeq$3800-9200 Å for $\sim 10^6$ galaxies to $r = 17.8$ and $\sim 10^5$ quasars to $i = 19.1$ ($i = 20.2$ for $z > 3$ candidates; Richards et al. 2002).

The $z_{em} = 2.062$ BAL quasar SDSS J024221.87+004912.6 (Schneider et al. 2002; Reichard et al. 2003; Schneider et al. 2005; Trump et al. 2006), hereafter referred to as SDSS J0242+0049, was observed spectroscopically three times by the SDSS (Table 1). We selected it for high-resolution spectroscopic followup because of the possible presence of narrow absorption in excited-state Si II and C II at $z = 2.042$. A spectrum obtained with the ESO Very Large Telescope (VLT) Unit 2 (Kueyen) and Ultra-Violet Echelle Spectrograph (UVES; Dekker et al. 2000) confirms the presence of narrow, low-ionization absorption at that redshift,[4] analysis of which will be reported elsewhere.

We observed SDSS J0242+0049 with UVES on the VLT UT2 on the nights of 4-5 September 2005 through a $1''$ slit with 2x2 binning of the CCD, yielding $R \simeq 40000$. The weather ranged from clear to thin cirrus, with $0.8 - 1.0''$ seeing. SDSS J0242+0049 was observed for a total of 5.75 hours in two different spectral settings, yielding coverage from 3291-7521 Å and 7665-9300 Å. Each exposure was reduced individually with optimum extraction (Horne 1986), including simultaneous background and sky subtraction. Telluric absorption lines were removed for the red settings using observations of telluric standard stars. A weighted co-addition of the three exposures of each spectral setting was performed with rejection of cosmic rays and known CCD artifacts. Finally, all settings were rebinned to a vacuum heliocentric wavelength scale, scaled in intensity by their overlap regions, and merged into a single spectrum with a constant wavelength interval of 0.08 Å (Figure 1). The SDSS spectra all share a common wavelength system with pixels equally spaced in velocity, and so for ease of comparison we created a version of the UVES spectrum binned to the those same wavelengths but not smoothed to the SDSS resolution.

3. BROAD ABSORPTION LINE TROUGH VELOCITY SHIFTS

The broadest absorption lines in SDSS J0242+0049 occur at a redshift $z \simeq 1.87988$ ($v = -18400 \, \mathrm{km \, s^{-1}}$ relative to the quasar) in Lyα, N V, Si IV and C IV (Figure 2). There is an offset between the peak absorption in C IV and Si IV. The redshift $z = 1.87988$ was determined from the deepest absorption in the Si IV trough, and does not match the deepest C IV absorption. This can be ascribed to a changing ionization state in the outflow as a function of velocity.

Comparison of the SDSS and UVES spectra suggested a shift in the position of the C IV trough at this redshift. To investigate further, continuum regions around that trough and the Si IV trough at the same redshift were fitted and used to normalize all observed spectra. (The Lyα and N V troughs lie outside the SDSS wavelength range.) For each epoch, the C IV and Si IV regions were fit separately with third order Legendre functions using SPLOT in IRAF.[5] The continuum sample windows were selected to avoid emission lines in the quasar rest frame (Vanden Berk et al. 2001).

The extent of any shift can be measured by minimizing the χ^2 between the normalized pixel-by-pixel fluxes in the spectra when shifted by an integer number of pixels m (assuming pixels equally spaced in velocity):

$$\chi^2_{\nu,m} = \frac{1}{N-m} \sum_{i=1}^{N-m} \frac{(f_{2,i} - f_{1,i+m})^2}{\sigma^2_{1,i} + \sigma^2_{2,i+m}} \qquad (1)$$

where $f_{2,i}$ and $f_{1,i+m}$ represent the flux in spectra from epochs 1 and 2 at pixels i and $i + m$, respectively, N is the total number of pixels extracted from each spectrum for comparison and σ is the error for the flux at each pixel.

The SDSS spectra from epochs 51821 and 52188[6] were compared with the UVES spectrum from epoch 53619 (Table 1). A clear shift was found in C IV and a potentially smaller shift in Si IV. Neither trough shows a detectable shift between the SDSS spectra from epoch 51821 and epoch 52188, and neither would be expected to do so if the observed long-term shift was due to a constant acceleration (the shift between those two epochs would be $\lesssim 0.5$ pixel for C IV). In light of this, the χ^2 test was conducted again, using a weighted average of all three SDSS spectra, with mean epoch 52066. From that comparison we conclude that the shift in C IV is 3 ± 1 pixels with 95.4% confidence (2σ). Zero velocity shift in C IV can be excluded with 99.9998% confidence. For Si IV, the shift is 1 ± 3 pixels at 95.4% confidence. Plots of these spectra are shown in the top two panels of Figure 3. It is important to note that there is no shift in the nearby narrow absorption lines. Also, both troughs appear to keep a relatively constant intensity, within the uncertainties. The bottom panel of Figure 3 shows the excellent match to the epoch 53619 UVES spectrum that

---

[4] The weak, narrow character of that absorption led to the classification of this object as a high-ionization BAL quasar by Reichard et al. (2003) and Trump et al. (2006) based on its SDSS spectrum.

[5] The Image Reduction and Analysis Facility (IRAF) is distributed by the National Optical Astronomy Observatories, which is operated by AURA, Inc., under contract to the National Science Foundation.

[6] Since the SDSS spectra from MJD 52177 and MJD 52199 are noisier at short wavelengths than the SDSS spectrum from MJD 51821 and since visual inspection of them revealed no obvious difference in their BAL troughs, a weighted co-add of their spectra was made, with mean epoch 52188.

results when the epoch 52066 average SDSS spectrum is shifted by 3 pixels.

The middle panel of Figure 3 may suggest that the long-wavelength end of the C IV trough has a greater shift than the short-wavelength end. Splitting the C IV trough into two sections, we find that χ^2 is minimized at a shift of 2^{+2}_{-1} pixels for the short-wavelength end and a shift of 4^{+1}_{-2} pixels for the long-wavelength edge, but that a uniform shift produces a marginally lower minimum overall χ^2. Thus, while there is possible evidence for a nonuniform velocity shift of the C IV BAL trough, the current data are of insufficient quality to prove its existence. Many physical effects could produce a nonuniform shift (expansion of an overpressured, accelerated shell of gas from an intermittent outflow, to give one example).

A shift of one SDSS pixel corresponds to a velocity shift of 69 km s^{-1} in the observed frame or 22.5 km s^{-1} in the quasar rest frame ($z = 2.062$). A shift of 3 ± 1 SDSS pixels (2σ) over a rest-frame time span of 1.39 years thus gives an acceleration of $a = 0.154 \pm 0.025$ cm s^{-2}, where the error is 1σ. Previously claimed accelerations for BAL troughs are much lower than that, at $a = 0.035 \pm 0.016$ cm s^{-2} over 5.5 rest-frame years in Q 1303+308 (Vilkoviskij & Irwin 2001) and $a = 0.08 \pm 0.03$ cm s^{-2} over 12 rest-frame years for Mrk 231 (Rupke et al. 2002). Our observation is more similar to that of Gabel et al. (2003), who determined the deceleration of C IV, N V and Si IV in a narrow absorption system in a Seyfert galaxy and found (for C IV) relatively large values of $a = -0.25 \pm 0.05$ cm s^{-2} and $a = -0.10 \pm 0.03$ cm s^{-2} over 0.75 and 1.1 rest-frame years, respectively. All of those observations involved much narrower troughs than is the case in SDSS J0242+0049. Also, the 1σ relative uncertainty associated with the acceleration of SDSS J0242+0049 is lower than the previous BAL measurements. These factors make SDSS J0242+0049 a robust case for line-of-sight acceleration of a true BAL trough. Still, it should be kept in mind that all these accelerations are much smaller than the $a \simeq 100$ cm s^{-2} predicted for the main acceleration phase of a disk wind in the model of Murray et al. (1995).

Furthermore, BAL troughs can vary for several reasons. These include acceleration or deceleration along the line of sight of some or all of the absorbing gas, a change in the ionization state of some or all of the gas, or a change in $C(v)$ — the covering factor of the gas as a function of the line-of-sight velocity — due to the movement of gas into or out of our line of sight, for example due to a change in flow geometry (see the introduction and §3.3 of Gabel et al. 2003). In many cases of variability all of the above origins are possible, but there are cases where acceleration is very unlikely to be the cause (see below). Because of this, to be conservative we cannot assume that BAL trough variability is due to acceleration even though acceleration *could* be the cause of much of the observed variability.

Fig. 2 of Barlow et al. (1989) and Fig. 2 of Barlow et al. (1992b) are cases where observed time variability of BAL troughs is almost certainly due to a change in the column densities of an ion at certain velocities (whether due to a changing ionization or to bulk motion into the line of sight), not due to a given ionic column density changing its velocity. More ambiguous cases are illustrated by C IV in Q 1246−057 (Fig. 3 of Smith & Penston 1988) and Si IV in Q 1413+117 (Fig. 15 of Turnshek et al. 1988). In both of those cases, a second-epoch spectrum shows more absorption at the short-wavelength edge of the trough in question. That could be because gas at lower outflow velocities in the trough was accelerated to higher velocities. Yet in both cases, the trough away from the short-wavelength edge is unchanged between the two epochs. If acceleration was the cause of the variability, a reduction in covering factor or optical depth, or both, might be expected at the lower velocities where the gas originated. No reduction is seen, arguing against the line-of-sight acceleration hypothesis for these cases of trough variability.

While every case for acceleration in a BAL trough will be ambiguous at some level, comparing the variability we report in SDSS J0242+0049 to previous cases leads us to believe that ours is the least ambiguous case seen to date of acceleration in a true BAL trough ($\gtrsim 1000$ km s^{-1} wide). Monitoring the future behavior of the $z = 1.87988$ absorption in this quasar would be very worthwhile, to see if the acceleration was temporary, is constant, increasing, or decreasing, or varies stochastically. The latter might occur if the velocity shift is due to a variable flow geometry or to ionization variations as a function of velocity caused by a fluctuating ionizing luminosity. (Recall from Figure 2 that this system shows some evidence for ionization stratification with velocity, in the form of an offset between the velocities of the peak Si IV and C IV absorption.) As this quasar is located in the equatorial stripe of the SDSS, which has been repeatedly imaged over the past 7 years, it should eventually be possible to search for a correlation between its ultraviolet luminosity and the acceleration of this system. (From the spectra alone, there appears to be a 5-10% increase in the luminosity of the object over the time spanned by the three SDSS spectra, but no information is available on longer timescales since the UVES spectrum is not spectrophotometrically calibrated.) BAL trough velocity shifts are also expected if BAL quasars are a short-lived phase during which material is expelled from the nuclear region (Voit, Weymann, & Korista 1993). In such a model the accelerating trough in SDSS J0242+0049 could be interpreted as gas unusually close to the quasar, currently experiencing an unusually large radiative acceleration.

4. OVERLAPPING SI IV TROUGHS

There is a possible case of line-locking involving Si IV in SDSS J0242+0049. Stable line-locking in a given doublet occurs when two conditions are met. First, the velocity separation between two absorption systems at different redshifts must be very nearly equal to the velocity separation of the two lines of a doublet seen in both systems (Braun & Milgrom 1989). Second, the reduction in line-driven acceleration of the shadowed system due to the reduced incident flux in one component of the doublet must result in its acceleration being the same as that of the shadowing system. This latter condition may be difficult to meet in AGN outflows, where many lines contribute to the radiative acceleration and there may also be substantial non-radiative acceleration. Nonetheless, some spectacular examples of apparent line-locking in AGN do suggest that it can in fact occur (e.g., Srianand et al. 2002), even if only rarely.

As shown in Figure 4, in SDSS J0242+0049 there is narrow Si IV absorption at $z = 2.0476$ (hereafter system A$'$) and a broad Si IV trough centered at about $z = 2.042$ (hereafter system A). Si IV line-locking of a third absorption system to system A$'$ or A would result in absorption 1931 km s^{-1} shortward of those redshifts, at $z = 2.0280$ or $z = 2.02245$ respectively. What is observed in the spectrum, however, is broad absorption in between the expected redshifts, centered at $z = 2.0254$ (hereafter system B). Both systems are observed in other transitions as well, with system B having more absorption in N V and C IV but less in S IV and Mg II.

In this section we consider first the optical depths and covering factors of these overlapping systems, with intriguing results. We then consider whether they could be line-locked or in the process of becoming line-locked.

4.1. *Si IV Trough Optical Depths and Covering Factors*

It is useful to determine if the Si IV troughs under consideration are optically thick or not. Figure 5 shows the absorption profiles in velocity space relative to $z = 2.0476$ or to the corresponding line-locked redshift of $z = 2.0280$. System A+A$'$, seen unblended in the bottom panel, is free from contamination in the blended trough (middle panel) at $-900 < v < -650$ km s^{-1}. At those velocities, absorption from the $\lambda1402$ component of System A+A$'$ (bottom panel) appears so similar in shape and intensity to absorption from the intrinsically stronger $\lambda1393$ component (middle panel) that we can conclude system A+A$'$ is optically thick in Si IV. For system B (seen unblended in the top panel) we must see how well various combinations of optical depth, covering factor, and geometry (Rupke, Veilleux, & Sanders 2005) can reproduce the profile of the trough composed of blended absorption from system B and the optically thick system A+A$'$ (middle panel).

For an unblended doublet, at each velocity v the normalized residual intensities I_1 and I_2 (in the stronger and weaker lines, respectively) can be related to the optical depth in the stronger transition τ and the fraction of the emitting source covered by the absorber along our line of sight, the covering factor C (e.g., Hall et al. 2003):

$$I_1(v) = 1 - C_v(1 - e^{-\tau_v}) \qquad (2)$$

$$I_2(v) = 1 - C_v(1 - e^{-R\tau_v}) \qquad (3)$$

where R measures the relative optical depths of the lines. For the Si IV $\lambda\lambda1393, 1402$ doublet, $R = 0.5$. In each absorption system we have only one unblended component, but it can still be used to model the other component. (For comparison, the two unblended troughs are overplotted on the blended trough in the top panel of Figure 6.)

First we test whether system B can be optically thin, with $C_v = 1$. Using this assumption and equations 2 and 3, the optical depth $\tau_v(\lambda1402, B)$ was calculated from the observed trough of Si IV $\lambda1393$ in system B. The blended trough profile in this model should be $\exp[-\tau_v(\lambda1402, B)]$ times the profile of Si IV $\lambda1393$ in system A+A$'$. (The latter profile is taken as identical to the $\lambda1402$ trough profile at $z = 2.0476$ since system A+A$'$ is optically thick.) The resulting model blended-trough profile is compared to the observed blended-trough profile in the second panel of Figure 6. Optically thin absorption from system B falls short of explaining the depth of the blended trough.

Next we test whether system B can be extremely optically thick, so that the depth of its absorption is determined only by C_v. In this case, we have two absorption systems absorbing at each v, but with different C_v. The total absorption is determined by $C_{v,blended}$, which depends on what parts of the emitting source(s) are covered by neither absorption system, by just one, or by both. That is, the total absorption depends on the extent to which the two systems overlap transverse to our line of sight and cover the same parts of the source. We can rule out the limit of minimum overlap, which yields maximum coverage of the source: $C_{v,blended} = \min(C_A + C_B, 1)$. In that case $C_A + C_B > 1$ at all v, but we do not observed $C_{v,blended} = 1$ at all v. Another limiting case is maximum overlap of the absorption systems, which minimumizes the source coverage: $C_{v,blended} = \max(C_A, C_B)$. The results of that model are shown in the third panel of Figure 6. It is not an improvement over the optically thin model. However, at almost all velocities the maximum-overlap model has more residual flux than seen in the data, while the minimum-overlap model has less. Thus, overlap in C_v which is less than the maximum possible by a velocity-dependent amount can explain the data. Such spatially-distinct, velocity-dependent partial covering has been seen before in other quasars (see the Appendix to Hall et al. 2003).

The last case we consider is one where each covering fraction describes the fractional coverage of the other absorption system as well as of the continuum source, so that $I_{v,blended} = I_A I_B$ and $C_{v,blended} = C_A + C_B - C_A C_B$ (this is case 3 of Rupke et al. 2005). The results of this model are shown in the bottom panel of Figure 6, again assuming A and B are both very optically thick. The model reproduces the data reasonably well at almost all velocities, and much more closely overall than the other models considered.

The good fit of this model implies that the absorption in one or both of the systems is produced by many small subunits scattered all over the continuum source from our point of view. In that case, the amount of light transmitted through both systems will naturally be $I_A(v) \times I_B(v)$ *at every velocity* v (Figure 7). Deviations will only occur due to statistical fluctuations, which will be greater the fewer subunits there are. It is more difficult, though still possible, to explain the observations using two 'monolithic' systems; that is, systems in which absorption from the ion in question arises in a single structure along our line of sight spanning the range of velocities seen in the trough, but with physical coverage of the source which varies with velocity (e.g., Figure 10 of Arav et al. 1999). Two monolithic flows with unblended residual intensities $I_A(v)$ and $I_B(v)$ can produce any blended residual intensity from 0 to $\min(I_A(v), I_B(v))$ essentially independently at each velocity v (Figure 7). Thus, two monolithic flows can explain the observations, but only if they just happen to overlap as a function of velocity in such a way as to mimic the overlap of two systems of clouds. Such an explanation is rather contrived, and we conclude instead that many small subunits exist in one or both absorption systems. This conclusion should of course be tested with observations of additional overlapping ab-

sorption systems in other quasars, to ensure this case is not a fluke.

Note that we have not considered the effects of different covering factors for the continuum source and broad emission line region. As seen in Figure 4, line emission is a 10% effect at best, and is not a factor at all in the Si IV $\lambda 1393$ trough of system B.

4.1.1. *Constraints on the Outflow Subunits*

The results above suggest that the absorbers A and B are composed of a number of optically thick subunits. We now discuss what we can infer about the parameters of these subunits, in the limit that each subunit is so optically thick it can be treated as opaque.

Assume that absorber A's residual intensity at some velocity, $I_A(v)$, is created by N_A subunits intercepting our line of sight, and similarly for absorber B. When the two absorbers overlap along the line of sight, there will be $N = N_A + N_B$ subunits along the line of sight. The average transmitted flux i in this case will be $<i> = (1-p)^N$, where p is the average fraction of the quasar's emission covered by an individual subunit.

If an average N over all velocities is well defined, the pixel-to-pixel variations around the average value $<i>$ will be distributed with variance $\sigma^2 = \sigma_I^2 + \sigma_i^2$, where σ_I is the instrumental error and σ_i is given by

$$\sigma_i^2 = \sigma_{intrinsic}^2 + (1-p)^{2N}\left(\frac{N^2\sigma_p^2}{(1-p)^2} + [\ln(1-p)]^2\sigma_N^2\right). \tag{4}$$

For example, fixed N at all velocities would have $\sigma_N^2 = 0$, while a Poisson distribution with an average of N would have $\sigma_N^2 = N$. The intrinsic variance at fixed N and p, $\sigma_{intrinsic}^2$, is caused by the random overlap (or lack thereof) of N subunits of uniform projected fractional area a. The relation between p and a, and the form of $\sigma_{intrinsic}^2$, depends on the shape of the subunits and of the quasar's emitting region. In the Appendix we give formulae for the cases of rectangular subunits of width a and unit length and of circular subunits of area a, under the approximation that the emitting region of the quasar is projected on the sky as a square of unit area and uniform surface brightness (see the discussion in the Appendix). In both cases, $\sigma_p^2 \propto \sigma_a^2$. If σ_a is negligible, there are two unknowns (a and N) and two observables ($<i>$ and σ) which can be used to solve for them.

More generally, we can constrain the subunit number and size as follows. We have a predicted profile $i(v) = I_A I_B$ and an observed profile $I(v)$, both of which depend on velocity. In our case, the wide range of i over the full trough and the smooth pixel-to-pixel distribution of i cannot simultaneously be reproduced at fixed N. Reproducing the wide range of i would require a small N, which would not generate as smooth a velocity profile as observed. Each subunit will probably have a velocity dispersion of only ~ 10 km s^{-1} (Peterson 1997), so for small N strong variations in i would be seen on that velocity scale. Thus, the range in i means either N or a varies with velocity, or both do. To simplify the problem, we assume the subunits have a uniform size so that a is constant and $\sigma_a = 0$. (This should be an adequate approximation if the subunits have a characteristic size scale.) If we then assume a value for a, we can calculate

a predicted N for each pixel as $N = \log i / \log(1-p)$, using the expression for $p(a)$ appropriate to the chosen geometry. The observed profile I differs slightly from the predicted profile $i = I_A I_B$, due to the intrinsic variance on the total covering factor of N clouds ($\sigma_{intrinsic}^2$) and to the errors on I_A and I_B (σ_A and σ_B, respectively). Setting $\sigma_p \propto \sigma_a = 0$ as discussed above and approximating the variance on N as $\sigma_N^2 = N$, we have

$$\sigma_i^2 \simeq \sigma_{intrinsic}^2 + (1-p)^{2N}N[\ln(1-p)]^2 + I_B^2\sigma_A^2 + I_A^2\sigma_B^2. \tag{5}$$

The probability of observing a residual intensity $I \pm \sigma_I$ in a pixel, given a predicted value i and associated σ_i, is

$$P(I \pm \sigma_I | i \pm \sigma_i) = \frac{1}{\sqrt{2\pi(\sigma_I^2 + \sigma_i^2)}} \exp\left[-\frac{(I-i)^2}{2(\sigma_I^2 + \sigma_i^2)}\right]. \tag{6}$$

Each pixel has a different σ_i which depends on the adopted a. To choose the best model, we find the value of a that maximizes the likelihood of the observations: $L = \prod_k P(I_k \pm \sigma_{I_k} | i_k \pm \sigma_{i_k})$. Note that a systematic error in I (e.g., due to a continuum estimate which is too high or too low) will yield a systematic error in a.

We use the velocity range $-700 < v < -75$ km s^{-1} to calculate L, avoiding both the narrow system A' and the high-velocity edge of the trough from system A where convolution with the instrumental line spread function may alter the true relative absorption depths in the two lines of a doublet (Ganguly et al. 1999). We find a best-fit relative filament width $w = 0.0135$, with a 99.994% (4σ) probability range of $0.0014 < w < 0.0430$. We find a best-fit relative cloud radius $r = 0.081$, with a 99.994% (4σ) probability range of $0.029 < r < 0.143$. There is no statistically significant difference between the likelihood of the two fits.

To convert these to physical sizes, we model the quasar's emission as being from a Shakura & Sunyaev (1973) accretion disk with viscosity parameter $\alpha = 0.1$ radiating at the Eddington limit. (We discuss the issue of coverage of the quasar's broad emission line region at the end of the section.) For this quasar we estimate $M_{BH} = 6.2 \times 10^8$ M$_\odot$ from the second moment of its Mg II emission line and its 3000 Å continuum luminosity, using the methods of Rafiee et al. (2007, in preparation). For those parameters, 99% of the continuum emission at rest-frame 1400 Å comes from $r < 150R_{Sch}$, where $R_{Sch} = 2GM_{BH}/c^2 = 1.8 \times 10^{14}$ cm is the Schwarzschild radius of the black hole. Since the relative sizes derived above were referenced to a square, not a circle, we adopt the square that has the same area as a circle with radius $150R_{Sch}$, which has sides of length $l = 4.8 \times 10^{16}$ cm. Thus, we find a best-fit filament width of $w = 6.5 \times 10^{14}$ cm, with a 4σ range of $6.7 \times 10^{13} < w < 2.1 \times 10^{15}$ cm, and a best-fit cloud radius $r = 3.9 \times 10^{15}$ cm, with a 4σ range of $1.4 \times 10^{15} < r < 6.9 \times 10^{15}$ cm.

These sizes, small on astronomical scales, suggest an origin for the subunits in the accretion disk for either geometry. A plausible length scale for structures originating in an accretion disk is the scale height h of its atmosphere (Equation 2.28 of Shakura & Sunyaev 1973).[7]

---

[7] If the accretion disk has a strong magnetic field, the pressure scale height may be a less plausible characteristic length. Numer-

At large radii, $h \simeq 3R^3 kT_s/4GM_{BH}m_p z_0$ where R is the distance from the black hole, T_s is the disk surface temperature and z_0 is the disk half-thickness. (Though not obvious from the above, $h < z_0$ because the disk surface temperature is lower than its midplane temperature.) In this object, the best-fit filament width equals the scale height h at $r = 5500R_{Sch} = 9.9 \times 10^{17}$ cm and the best-fit cloud radius equals the scale height h at $r = 25000R_{Sch} = 4.5 \times 10^{18}$ cm. The various parameters for our two geometries are summarized in Table 2.

Strikingly, the first of those distances from the central source is equal to the distance the absorber must have to cover the emission from the quasar's broad emission line region (BELR). As seen in Figure 4, the line emission in the region of the absorption troughs reaches at most 10% of the continuum level, and at least system A covers both the continuum emission region and the Si IV/O IV] BELR. In other transitions, both systems at least partially cover the N V and C IV BELRs, and at least system A covers the Mg II BELR. Since AGN BELRs are stratified, with lower-ionization gas located farther from the quasar, to be conservative we assume both systems lie exterior to the Mg II BELR in SDSS J0242+0049. We use a relationship between $L_\lambda(3000\text{\AA})$ and $R_{\text{BELR,MgII}}$ derived from reverberation-mapping data (Peterson et al. 2004; Rafiee et al. 2007, in preparation) to obtain $R_{\text{BELR,MgII}} = 9.1 \times 10^{17}$ cm $= 5000R_{Sch}$ for SDSS J0242+0049. Given the $\pm 25\%$ 1σ scatter in this relationship, this distance is in excellent agreement with the distance required for filamentary absorber subunits to have widths matching the disk scale height. Of course, the absorber could be located at any $R > R_{\text{BELR,MgII}}$, so spherical clouds of size equal to the disk scale height could still match the data if the outflow arises at sufficiently large radii.

We have outlined a consistent picture wherein systems A and B, whether they consist of opaque filaments or clouds, are launched from the accretion disk exterior to the Mg II BELR with a subunit size comparable to the scale height of the accretion disk atmosphere at that radius. As a system accelerates, its typical density will decrease and its typical ionization will increase, explaining the presence of high ionization species in flows arising from a low-ionization emission-line region. When the systems cross our line of sight, they have line-of-sight velocities of $v_{los} = -2000\,\text{km\,s}^{-1}$ for system A and $v_{los} = -3600\,\text{km\,s}^{-1}$ for system B. For System A, $|v_{los}|$ is comparable to the $v_{orbital} = 2900\,\text{km\,s}^{-1}$ expected at its inferred launch radius of $5500R_{Sch}$. For System B, $|v_{los}|$ is larger than the $v_{orbital} = 1400\,\text{km\,s}^{-1}$ expected at its inferred launch radius of $25000R_{Sch}$. The spherical cloud dispersal time would be of order ~ 110 years for $T \sim 10^4$ K, so the subunits will not disperse on their own between launch and crossing our line of sight. However, partial shadowing of a subunit will produce differential radiative acceleration of the subunit. Substantial radiative acceleration could thus shorten the subunit lifetimes considerably.

One potential complication is that the observed profile of the overlapping trough deviates from the multiplica-

ical simulations of accretion disks do not yet conclusively show if another characteristic scale is produced by magnetohydrodynamic turbulence (Armitage 2004).

tive prediction (Figure 6, bottom panel) in a manner that is not random on velocity scales larger than $\sim 10\,\text{km\,s}^{-1}$. However, deviations on such scales should be random if, as expected, the individual subunits have velocity dispersions of that order. Instead, the deviations seem to be coherent on $\sim 100\,\text{km\,s}^{-1}$ scales. It may be that the subunits do have velocity widths of that order due to microturbulence (Bottorff et al. 2000). Another possible explanation is that the outflow consists of filaments wherein the material is accelerated so that its line-of-sight velocity increases by $\sim 100\,\text{km\,s}^{-1}$ as it crosses the line of sight (e.g., Arav et al. 1999). Deviations from the expected profile should then persist for $\sim 100\,\text{km\,s}^{-1}$ instead of $\sim 10\,\text{km\,s}^{-1}$. As compared to a model without line-of-sight acceleration, there could be the same average number of filaments, but the number would change more slowly with velocity (although other effects, such as filaments not being exactly parallel, can affect that as well). Observations of additional overlapping systems would be useful for investigating this issue.

We note that Goodman (2003) have shown that thin accretion disks without winds will be unstable to self-gravity beyond $r_{Q=1} \simeq 2740(10^8 \alpha l_E^2/M_{BH})^{2/9} R_{Sch}$ where l_E is the Eddington ratio; using the parameters adopted herein, SDSS J0242+0049 has $r_{Q=1} \simeq 1100R_{Sch}$. However, removal of angular momentum by a disk wind might help stabilize a thin disk (§4.3 of Goodman 2003), and there is reason to believe such a process operates in AGN. Reverberation mapping places the BELRs of many AGN at $r > r_{Q=1}$, and there is evidence that BELRs are flattened (Vestergaard, Wilkes, & Barthel 2000; Smith et al. 2005; Aars et al. 2005) as expected if they are located at the bases of accretion disk winds (Murray et al. 1995). Furthermore, quasar spectral energy distributions are consistent with marginally gravitationally stable disks extending out to $\sim 10^5 R_{Sch}$ (Sirko & Goodman 2003).

Lastly, we note that there is no contradiction in using the continuum source size to derive the scale size of the subunits for an outflow the size of the BELR. This is because the continuum source has a surface brightness $\simeq 2100$ times that of the BELR. That number is the ratio of the continuum flux near $1400\,\text{\AA}$ in SDSS J0242+0049 to the Si IV/O IV] flux, which we take to be $\simeq 9$, times the ratio of the areas of the Si IV/O IV] BELR and the $1400\,\text{\AA}$ continuum source.[8] If N subunits of the absorber each cover a fractional area a of the continuum source, Nx subunits of the absorber will each cover a fractional area a/x of the BELR. For large N and small a the residual intensity of each region is equal, $i = (1-a)^N \simeq (1-a/x)^{Nx}$, but the variance on i from the BELR will be a factor $\simeq 0.1/x$ smaller than the variance on i from the continuum source. Thus, an absorber covering both the continuum source and BELR will have essentially the same residual intensity i and variance σ_i^2 (used to derive the absorber size constraints via Equation 6) as an absorber covering only the continuum source.

[8] The size of the Si IV/O IV] BELR has been measured in only three AGN (Peterson et al. 2004). On average, it is comparable in size to the C IV BELR. We therefore use the relationship between $L_\lambda(1350\text{\AA})$ and $R_{\text{BELR,CIV}}$ given by Peterson et al. (2006) to derive $R_{\text{BELR,SiIV}} = 4.1 \times 10^{17}$ cm for SDSS J0242+0049.

4.2. *Possible Si IV Line-Locking*

We now return to the issue of whether systems A+A′ and B can be line-locked. Line-locking occurs when the reduction in line-driving flux caused by the shadow of one system decelerates the other, shadowed system so that two systems end up with the same acceleration (which may be nonzero). The two systems thereafter maintain a constant velocity separation that keeps one system shadowed (Braun & Milgrom 1989). (However, there is some debate in the literature as to whether line-driven winds are unstable to the growth of shocks (Owocki, Castor, & Rybicki 1988; Pereyra et al. 2004). If shocks can develop, they could accelerate the wind out of an otherwise stable line-locking configuration.) For line-locking to occur in an accelerating flow, there are two possibilities. System B could have appeared along a sightline linking the continuum source and system A+A′ at $2.0280 < z < 2.0476$ and accelerated until it reached $z = 2.0280$ and overlapped system A+A′ at $z = 2.0476$. Alternatively, system A+A′ could have appeared at $z > 2.0476$ and accelerated until it reached $z = 2.02476$ and overlapped system B at $z = 2.0280$.

The latter scenario can be ruled out because the greatest deceleration of system A+A′ would have occurred before it reached $z = 2.0476$, when it was shadowed by the deepest part of system B. Instead, the deepest part of system B is observed to be shadowed by the shallowest part of system A. If line-locking was going to occur in this scenario it would have had to set in when the shadowing was greatest (or earlier than that, if less than full shadowing produced sufficient deceleration). If it did not happen then, it will not happen with the observed, lesser amount of shadowing.

The former scenario of an accelerating system B which has ended up line-locked is plausible. The observed shadowing as a function of velocity could in principle have halted system B.

One requirement of this former scenario, however, is that the narrow absorption at $z = 2.0476$ (system A′) should not be associated with system A, the broad absorption immediately shortwards of it. If they were associated, then some of the gas in system B at $-350 < z < -50$ km s^{-1} should have come to a halt at 0 km s^{-1}, where the shadowing by system A′ would have been greater than the current shadowing by system A. System A′ must be located farther from the quasar than either system A or B, in this scenario.

The optically thickest part of system A is likely at $-650 < v < -450$ km s^{-1}, where numerous low-ionization species are seen. If any gas in system B was observed at $v < -650$ km s^{-1}, that gas would have passed the point of maximum shadowing without becoming line-locked. In fact, no gas in system B is seen at $v < -650$ km s^{-1}, consistent with system B being line-locked. One argument against this scenario is that if system B has been halted by the observed shadowing, gas at different velocities in that system has been halted by different amounts of shadowing. For example, gas at -200 km s^{-1} has been halted by shadowing of only $\sim$30% of the continuum, while gas at -450 km s^{-1} has been halted by shadowing of $\sim$95% of the continuum. It may be more physically plausible to suggest that gas at -450 km s^{-1} has been halted, but that gas at -200 km s^{-1} has not

yet been sufficiently shadowed to become line-locked. In other words, in this model system B is in the process of becoming line-locked. However, comparison of the SDSS and UVES spectra shows no evidence for variability in these Si IV troughs. The timescale for velocity changes in this scenario could be longer than 1.4 years (rest-frame), which would rule out line locking in a Murray et al. (1995) disk wind in which the entire acceleration phase lasts $\sim$ 1.6 years, or the line-locking could be occurring in a helical flow, stable on timescales of years, in which our sightline intercepts the flow before the gas becomes line-locked.

Finally, note that the Si IV profiles in SDSS J0242+0049 are intriguingly similar to some of the potentially line-locked N V profiles seen in RX J1230.8+0115 (Ganguly et al. 2003). The $z = 0.1058$ system in that object has a profile similar to that of system A+A′ (strongest absorption at both ends of the profile), and its $z = 0.1093$ system is similar to that of system B (optically thick, with the strongest absorption in the middle of the profile, at a velocity corresponding to the weakest absorption in the other system). Both systems have only about half the velocity widths of those in SDSS J0242+0049, however, and the relative velocities of the two systems are reversed — the weaker, single-peaked absorption profile has the lower outflow velocity. It is also worth noting that the Lyα absorption profile in each object appears to share the same covering factor as the species discussed above, while at least one moderately higher-ionization species in each object (N V here, and O VI in RX J1230.8+0115) has a larger covering factor which yields nearly black absorption troughs. Whether these similarities are just coincidences will require data on more candidate line-locking systems. (The line-locked systems in Q 1511+091 studied by Srianand et al. (2002) are much more complex, but do not seem to include any profiles similar to those in SDSS J0242+0049.)

5. CONCLUSIONS

We find that the C IV BAL trough at $z = 1.87988$ in the spectrum of SDSS J0242+0049 ($v = -18400$ km s^{-1} relative to the quasar's rest frame) has likely undergone an acceleration of $a = 0.154 \pm 0.025$ cm s^{-2} over a period of 1.39 rest-frame years. This is the largest acceleration yet reported in a BAL trough $\geq$1000 km s^{-1} wide.

We also derive constraints on the outflow properties of two absorption systems, overlapping and possibly line-locked in Si IV, at $z = 2.0420$ and $z = 2.0254$ ($v = -2000$ km s^{-1} and $v = -3600$ km s^{-1} relative to the quasar, respectively). The overlapping trough in common to both systems indicates that at least one of the systems must consist of individual subunits. This contrasts with results strongly suggesting that the BELR itself consists of a smooth flow, rather than a clumped one (Laor et al. 2006), but agrees with results for a narrow intrinsic absorber in the gravitational lens RXS J1131−1231 (Sluse et al. 2007).

Assuming identical, opaque subunits, our data are consistent with spherical clouds of radius $r \simeq 3.9 \times 10^{15}$ cm or linear filaments of width $w \simeq 6.5 \times 10^{14}$ cm. These subunits must be located at or beyond the Mg II broad emission line region. At that distance, the above filament width is equal to the predicted scale height of the outer atmosphere of a thin accretion disk. Insofar as that

is a natural length scale for structures originating in an accretion disk, these observations are evidence that the accretion disk is the source of the absorption systems. It would be useful to obtain high-resolution spectra of additional cases of distinct but overlapping intrinsic absorption troughs in quasar spectra to determine if this case is representative. If so, it would also be worth extending this work's analytic study of the implications of the residual intensity variance to numerical studies including a realistic quasar geometry, a range in absorber sizes and optical depths, etc.

APPENDIX

Consider the case of an absorber consisting of opaque subunits of a uniform shape. Suppose our line of sight to a quasar's emitting regions is intercepted by N of these subunits, randomly distributed transverse to the line of sight. Then the scatter possible in the covering fraction at fixed N due to the random overlap (or lack thereof) of the subunits with each other will depend on the shape of the subunits. To obtain expressions for this variance, we approximate the quasar's emitting regions as a square of uniform surface brightness on the plane of the sky. We do this solely because expressions for the variance have been derived for the case of the unit square covered by two relevant subunit geometries: circles of area a and filaments of unit length and width a. We take the first case to represent a true cloud model, and the second to represent a magnetically confined 'filament' model.

The case of the unit square randomly overlapped by filaments parallel to each other and to two sides of the square, and of unit length and width a, is treated by Robbins (1944). The unit square is defined as the set of points $\{0 \leq x \leq 1; 0 \leq y \leq 1\}$. The filaments that overlap the square are centered at $y = 0.5$ and distributed randomly in x over $-\frac{a}{2} \leq x \leq 1 + \frac{a}{2}$. Because of edge effects, the average area covered by a filament is $p = \frac{a}{1+a}$, and the average area uncovered by N filaments is $i = (1 - p)^N$. The variance in the fractional area covered is

$$\sigma^2_{\text{filaments}} = (1-a)^2(1-2p)^N - (1-p)^{2N} + \frac{2a[(1-p)^{N+1} - (1-a)(1-2p)^{N+1}]}{(N+1)p}$$
$$-\frac{2a^2[(1-p)^{N+2} - (1-2p)^{N+2}]}{(N+1)(N+2)p^2} \tag{1}$$

for $a < 0.5$.

In the case of the unit square randomly overlapped by circles of area a, circles that overlap the square are distributed such that their centers are within a distance $r = \sqrt{a/\pi}$ of the unit square. Again the average area uncovered by N circles is given by $i = (1 - p)^N$, but in this case $p = \pi r^2/(1 + 4r + \pi r^2)$. The variance in the fractional area covered can be derived from expressions given by Kendall & Moran (1963), yielding

$$\sigma^2_{\text{circles}} = \left[\frac{1 + 4r - \pi r^2}{1 + 4r + \pi r^2}\right]^N \left(1 - 4\pi r^2 + \frac{64}{3}r^3 - 8r^4\right) - \left(\frac{1 + 4r}{1 + 4r + \pi r^2}\right)^{2N}$$
$$+ 2\int_0^{2r} \left[1 - \frac{2r^2(\pi - \cos^{-1}\frac{q}{2r} + \frac{q}{2r}\sin\left(\cos^{-1}\frac{q}{2r}\right))}{1 + 4r + \pi r^2}\right]^N (\pi q - 4q^2 + q^3)\, dq \tag{2}$$

for $a < 0.5$. The integral must be evaluated numerically for most N.

For the same a and N, $\sigma^2_{\text{circles}} > \sigma^2_{\text{filaments}}$. This can be understood by placing a subunit of either type in the center of the square and considering the probability that a second subunit of the same type will overlap the first. There is an area $2a$ in which a second filament can be placed to have some overlap with the first (filament centers at $0.5 - a < x < 0.5 + a$). There is an area $4a$ in which a second circle can be placed to have some overlap with the first (circles centered within $2\sqrt{\frac{a}{\pi}}$ of $\{0.5, 0.5\}$, for an area of $\pi(2\sqrt{\frac{a}{\pi}})^2 = 4a$). If a is small, the most likely value of i is $i = 1 - 2a$ for both geometries, but with circles there is a higher probability of $i > 1 - 2a$ and thus a larger variance.

REFERENCES

Aars, C. E., Hough, D. H., Yu, L. H., Linick, J. P., Beyer, P. J., Vermeulen, R. C., & Readhead, A. C. S. 2005, AJ, 130, 23

Arav, N., Korista, K. T., de Kool, M., Junkkarinen, V. T., & Begelman, M. C. 1999, ApJ, 516, 27

Armitage, P. J. 2004, Theory of Disk Accretion onto Supermassive Black Holes (ASSL Vol. 308: Supermassive Black Holes in the Distant Universe), 89

Barlow, T., Hamann, F., & Sargent, W. 1997, in ASP Conf. Ser. 128: Mass Ejection from Active Galactic Nuclei, 13

Barlow, T., Junkkarinen, V., & Burbidge, E. 1989, ApJ, 347, 674

Barlow, T., Junkkarinen, V., & Burbidge, E. 1992a, in American Astronomical Society Meeting, Vol. 181, 1106

Barlow, T., Junkkarinen, V., Burbidge, E., Weymann, R., Morris, S., & Korista, K. 1992b, ApJ, 397, 81

Barlow, T. A. 1994, PASP, 106, 548

Bottorff, M. C., Ferland, G. J., Baldwin, J., Korista, K. 2000, ApJ, 542, 644

Braun, E. & Milgrom, M. 1989, ApJ, 342, 100

Bromage, G., Boksenberg, A., Clavel, J., Elvius, A., Penston, M., Perola, G., Pettini, M., Snijders, M., et al. 1985, MNRAS, 215, 1

Dekker, H., D'Odorico, S., Kaufer, A., Delabre, B., & Kotzlowski, H. 2000, in Proc. SPIE Vol. 4008, Optical and IR Telescope Instrumentation and Detectors, ed. M. Iye & A. Moorwood, 534

Foltz, C. B., Weymann, R. J., Morris, S. L., & Turnshek, D. A. 1987, ApJ, 317, 450

Fukugita, M., Ichikawa, T., Gunn, J. E., Doi, M., Shimasaku, K., & Schneider, D. P. 1996, AJ, 111, 1748

Gabel, J. R., Crenshaw, D. M., Kraemer, S. B., Brandt, W. N., George, I. M., Hamann, F. W., Kaiser, M. E., Kaspi, S., et al. 2003, ApJ, 595, 120

Gallagher, S. C., Brandt, W. N., Wills, B. J., Charlton, J. C., Chartas, G., & Laor, A. 2004, ApJ, 603, 425

Gallagher, S. C., Schmidt, G. D., Smith, P. S., Brandt, W. N., Chartas, G., Hylton, S., Hines, D. C., & Brotherton, M. S. 2005, ApJ, 633, 71

Ganguly, R., Charlton, J. C., & Eracleous, M. 2001, ApJ, 556, L7

Ganguly, R., Eracleous, M., Charlton, J. C., & Churchill, C. W. 1999, AJ, 117, 2594

Ganguly, R., Masiero, J., Charlton, J. C., & Sembach, K. R. 2003, ApJ, 598, 922

Goodman, J. 2003, MNRAS, 339, 937

Gunn, J., Siegmund, W., Mannery, E., Owen, R., Hull, C., Leger, R., Carey, L., Knapp, G., et al. 2006, AJ, 131, 2332

Gunn, J. E., Carr, M., Rockosi, C., Sekiguchi, M., Berry, K., Elms, B., de Haas, E., Ivezić , Ž., et al. 1998, AJ, 116, 3040

Hall, P. B., Anderson, S., Strauss, M., York, D., Richards, G., Fan, X., Knapp, G., Schneider, D., et al. 2002, ApJS, 141, 267

Hall, P. B., Hutsemékers, D., Anderson, S. F., Brinkmann, J., Fan, X., Schneider, D. P., & York, D. G. 2003, ApJ, 593, 189

Hamann, F., Barlow, T., Cohen, R., Junkkarinen, V., & Burbidge, E. 1997a, in Mass Ejection from Active Galactic Nuclei, ed. N. Arav, I. Shlosman, & R. Weymann (San Francisco: ASP), 19

Hamann, F., Barlow, T., & Junkkarinen, V. 1997b, ApJ, 478, 87

Hamann, F., Barlow, T. A., Beaver, E. A., Burbidge, E. M., Cohen, R. D., Junkkarinen, V., & Lyons, R. 1995, ApJ, 443, 606

Hogg, D., Finkbeiner, D., Schlegel, D., & Gunn, J. 2001, AJ, 122, 2129

Horne, K. 1986, PASP, 98, 609

Ivezić, Ž., Lupton, R., Schlegel, D., Boroski, B., Adelman-McCarthy, J., Yanny, B., Kent, S., Stoughton, C., et al. 2004, AN, 325, 583

Kendall, M. G. & Moran, P. A. P. 1963, Geometrical Probability (New York: Hafner), 112

Koratkar, A., Goad, M., O'Brien, P., Salamanca, I., Wanders, I., Axon, D., Crenshaw, D., Robinson, A., et al. 1996, ApJ, 470, 378

Laor, A., Barth, A., Ho, L., & Filippenko, A. 2006, ApJ, 636, 83

Leighly, K. M., Casebeer, D. A., Hamann, F., & Grupe, D. 2005, in Bulletin of the American Astronomical Society, 1184

Ma, F. 2002, MNRAS, 335, L99

Michalitsianos, A. G., Oliversen, R. J., & Nichols, J. 1996, ApJ, 461, 593

Misawa, T., Eracleous, M., Charlton, J. C., & Tajitsu, A. 2005, ApJ, 629, 115

Murray, N., Chiang, J., Grossman, S., & Voit, G. 1995, ApJ, 451, 498

Owocki, S. P., Castor, J. I., & Rybicki, G. B. 1988, ApJ, 335, 914

Pereyra, N. A., Owocki, S. P., Hillier, D. J., & Turnshek, D. A. 2004, ApJ, 608, 454

Peterson, B., Bentz, M., Desroches, L.-B., Filippenko, A., Ho, L., Kaspi, S., Laor, A., Maoz, D., et al. 2006, ApJ, 641, 638

Peterson, B., Ferrarese, L., Gilbert, K., Kaspi, S., Malkan, M., Maoz, D., Merritt, D., Netzer, H., et al. 2004, ApJ, 613, 682

Peterson, B. M. 1997, Active Galactic Nuclei (Cambridge: Cambridge University Press), 71–89

Pier, J. R., Munn, J. A., Hindsley, R. B., Hennessy, G. S., Kent, S. M., Lupton, R. H., & Ivezić, Ž. 2003, AJ, 125, 1559

Reichard, T., Richards, G., Schneider, D., Hall, P., Tolea, A., Krolik, J., Tsvetanov, Z., Vanden Berk, D., et al. 2003, AJ, 125, 1711

Richards, G., Fan, X., Newberg, H., Strauss, M., Vanden Berk, D., Schneider, D., Yanny, B., Boucher, A., et al. 2002, AJ, 123, 2945

Robbins, H. E. 1944, Annals of Mathematical Statistics, 15, 70

Rupke, D. S., Veilleux, S., & Sanders, D. B. 2002, ApJ, 570, 588

—. 2005, ApJS, 160, 87

Schneider, D. P., Hall, P. B., Richards, G. T., Vanden Berk, D. E., Anderson, S. F., Fan, X., Jester, S., Stoughton, C., et al. 2005, AJ, 130, 367

Schneider, D. P., Richards, G. T., Fan, X., Hall, P. B., Strauss, M. A., Vanden Berk, D. E., Gunn, J. E., Newberg, H. J., et al. 2002, AJ, 123, 567

Shakura, N. I. & Sunyaev, R. A. 1973, A&A, 24, 337

Sirko, E. & Goodman, J. 2003, MNRAS, 341, 501

Sluse, D., Claeskens, J.-F., Hutsemékers, D., & Surdej, J., A&A, in press (astro-ph/0703030)

Smith, J., Tucker, D., Kent, S., Richmond, M., Fukugita, M., Ichikawa, T., Ichikawa, S., Jorgensen, A., et al. 2002, AJ, 123, 2121

Smith, J. E., Robinson, A., Young, S., Axon, D. J., & Corbett, E. A. 2005, MNRAS, 359, 846

Smith, L. J. & Penston, M. V. 1988, MNRAS, 235, 551

Srianand, R., Petitjean, P., Ledoux, C., & Hazard, C. 2002, MNRAS, 336, 753

Trump, J., Hall, P., Reichard, T., Richards, G., Schneider, D., Vanden Berk, D., Knapp, G., Anderson, S., et al. 2006, ApJS, 165, 1

Turnshek, D. A., Grillmair, C. J., Foltz, C. B., & Weymann, R. J. 1988, ApJ, 325, 651

Vanden Berk, D. E., Richards, G. T., Bauer, A., Strauss, M. A., Schneider, D. P., Heckman, T. M., York, D. G., Hall, P. B., et al. 2001, AJ, 122, 549

Vestergaard, M., Wilkes, B. J., & Barthel, P. D. 2000, ApJ, 538, L103

Vilkoviskij, E. Y. & Irwin, M. J. 2001, MNRAS, 321, 4

Voit, G. M., Shull, J. M., & Begelman, M. C. 1987, ApJ, 316, 573

Voit, G. M., Weymann, R. J., & Korista, K. T. 1993, ApJ, 413, 95

York, D., Adelman, J., Anderson, J., Anderson, S., Annis, J., Bahcall, N., Bakken, J., Barkhouser, R., et al. 2000, AJ, 120, 1579

TABLE 1
SDSS J0242+0049 Spectroscopic Observations and Inferences

Source	SDSS Plate	SDSS Fiber	Epoch in MJD	Δt_{rest} (days)	Si IV, C IV Shift vs. MJD 52188	Si IV, C IV Shift vs. MJD 53619
SDSS (1)	408	576	51821	-80	0, 0	1, 4
SDSS (2)	707	332	52177	36	—	—
SDSS (3)	706	617	52199	43	—	—
SDSS Avg. (2+3)	—	—	(52188)	40	—	1, 3
SDSS Avg. (1+2+3)	—	—	(52066)	0	—	1, 3
UVES	—	—	53619	507	1, 3	—

Note. — Epochs are given on the Modified Julian Day (MJD) system. The *rest-frame* time interval Δt_{rest} is given relative to MJD 52066. Velocity shifts of absorption lines are given in SDSS pixels (69 km s^{-1}); the C IV shift is the first number and the Si IV shift is the second number.

TABLE 2
SDSS J0242+0049 Subunit Parameters

Subunit Geometry	Avg. Number of Subunits $\bar{N}$	Best-fit Relative Width or Radius	Relative 99.994% Confidence range	Best-fit Physical Width or Radius	Physical 99.994% Confidence range (cm)	Atmospheric Scale Height Distance
Filaments	203 ± 81	0.0135	$0.0014 - 0.0430$	6.5×10^{14} cm	$6.7 \times 10^{13} - 2.1 \times 10^{15}$	9.9×10^{17} cm $= 5500~R_{Sch}$
Spheres	177 ± 71	0.081	$0.029 - 0.143$	3.9×10^{15} cm	$1.4 \times 10^{15} - 6.9 \times 10^{15}$	4.5×10^{18} cm $= 25000~R_{Sch}$

Note. — The average number of subunits $\bar{N}$ is the number of subunits responsible for absorption at each pixel, averaged over all pixels. The total number of subunits present depends on the unknown velocity width of each subunit. The atmospheric scale height distance is the distance from the black hole at which the accretion disk atmospheric scale height equals the best-fit width or radius of the subunit in question; see §4.1. R_{Sch} refers to the Schwarzschild radius of a black hole with mass 6.2×10^8 M$_\odot$.
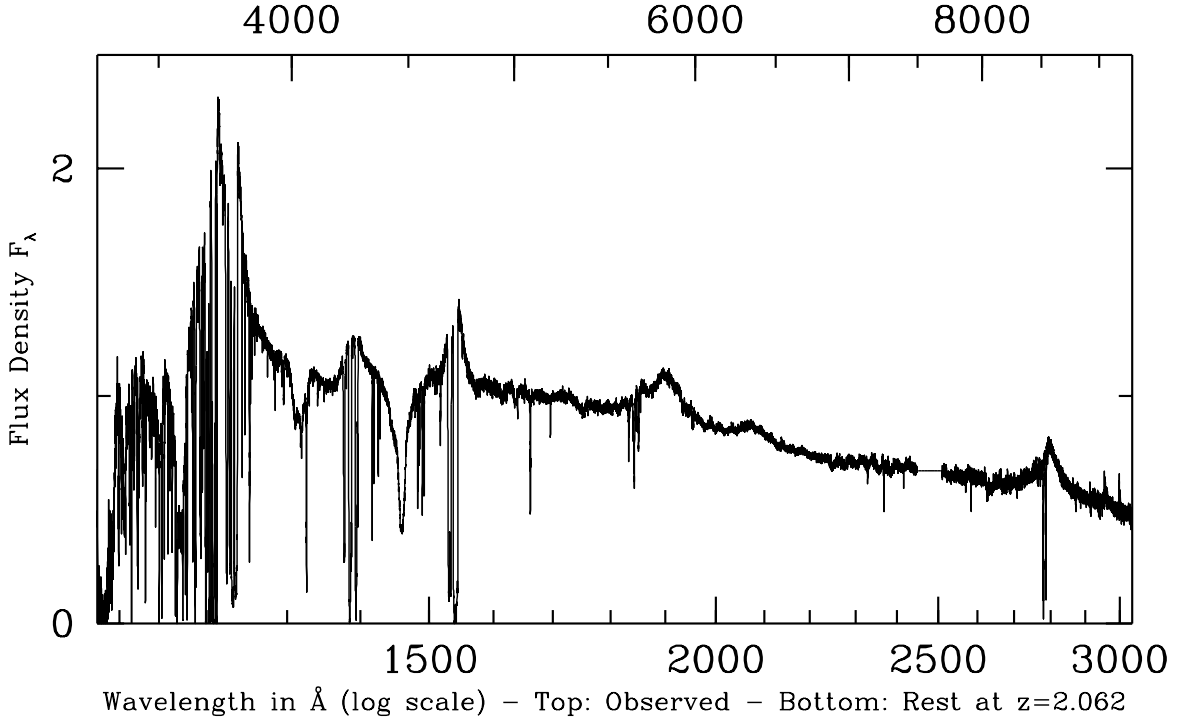

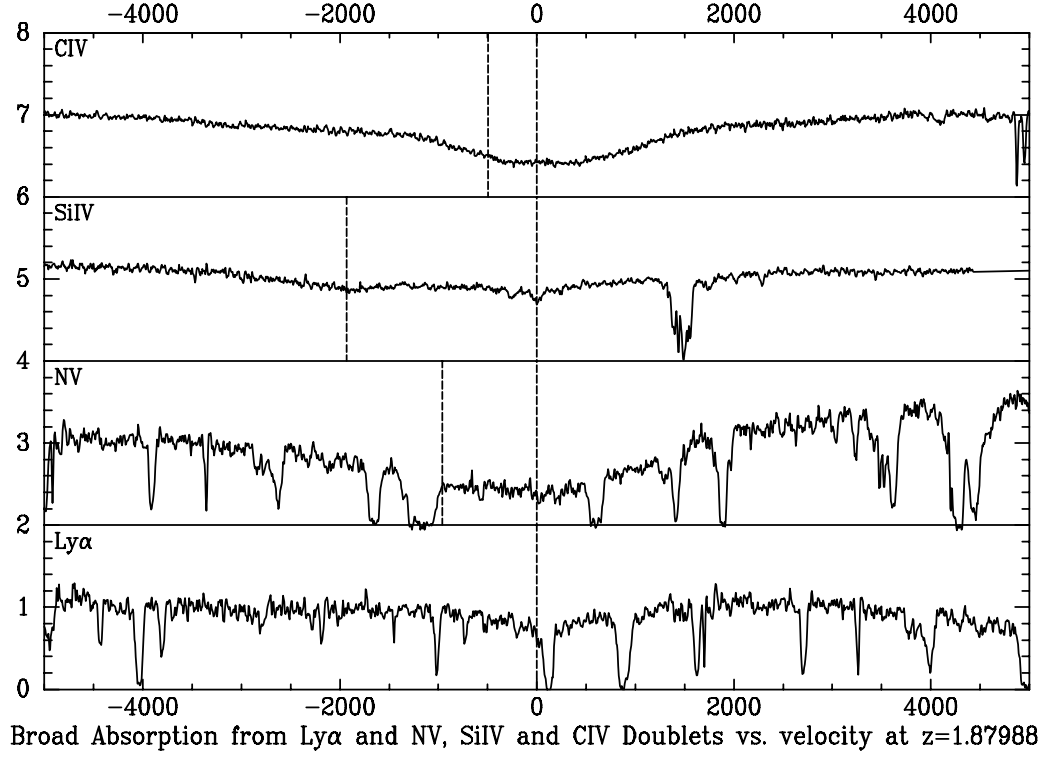Fig. 1.— VLT UT2 + UVES spectrum of SDSS J0242+0049, smoothed by a 1 Å boxcar filter.

FIG. 2.— UVES spectra of BAL troughs in SDSS J0242+0049 vs. velocity (in $km\,s^{-1}$) in the $z = 1.87988$ frame. Negative velocities indicate blueshifts and positive velocities indicate redshifts relative to that frame. Zero velocity corresponds to the long-wavelength members of doublets, and dashed vertical lines indicate all components of each transition. Contaminating narrow absorption lines are present near all troughs, but especially in those found shortward of the Lyα forest.
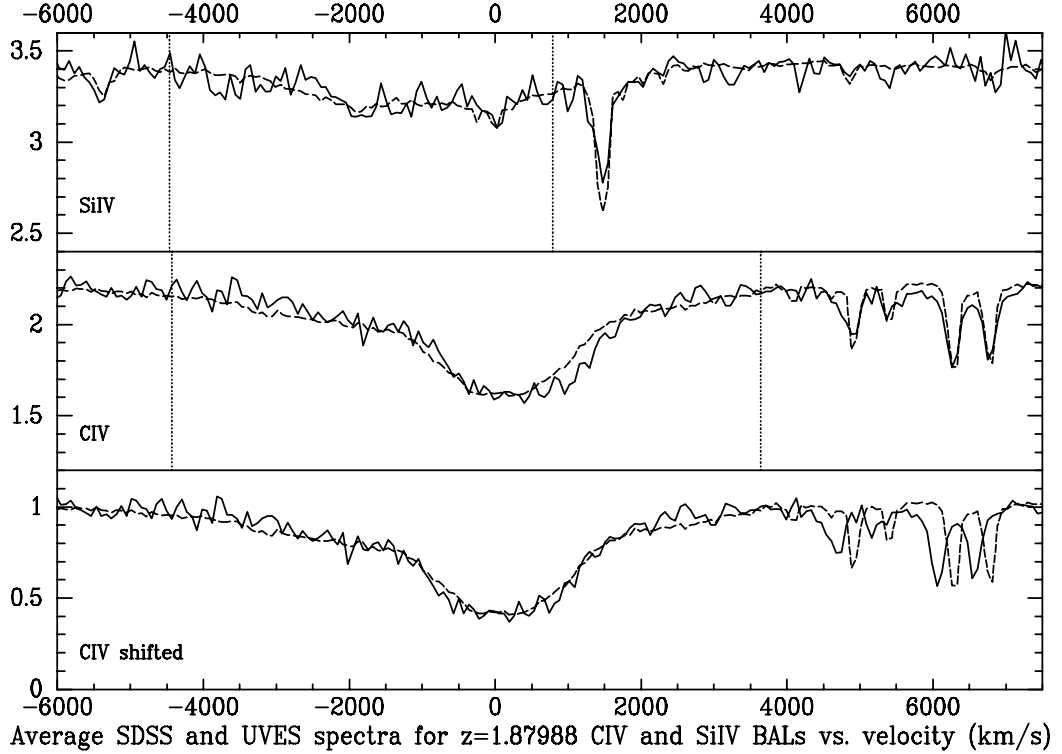

FIG. 3.— Comparison of the $z = 1.87988$ C IV BAL in SDSS J0242+0049 at the average SDSS epoch and the UVES epoch. Negative velocities indicate blueshifts and positive velocities redshifts, relative to $z = 1.87988$. The solid line is a weighted average of all three SDSS spectra. The dashed line is the UVES spectrum binned into the same pixels as the SDSS spectra. Dotted vertical lines indicate the fitting regions used when conducting the χ^2 test. The top panel compares the unshifted spectra for the Si IV trough, and the middle panel the unshifted spectra for the C IV trough. The bottom panel compares the C IV troughs after shifting the average SDSS spectrum toward shorter wavelengths by 3 pixels.
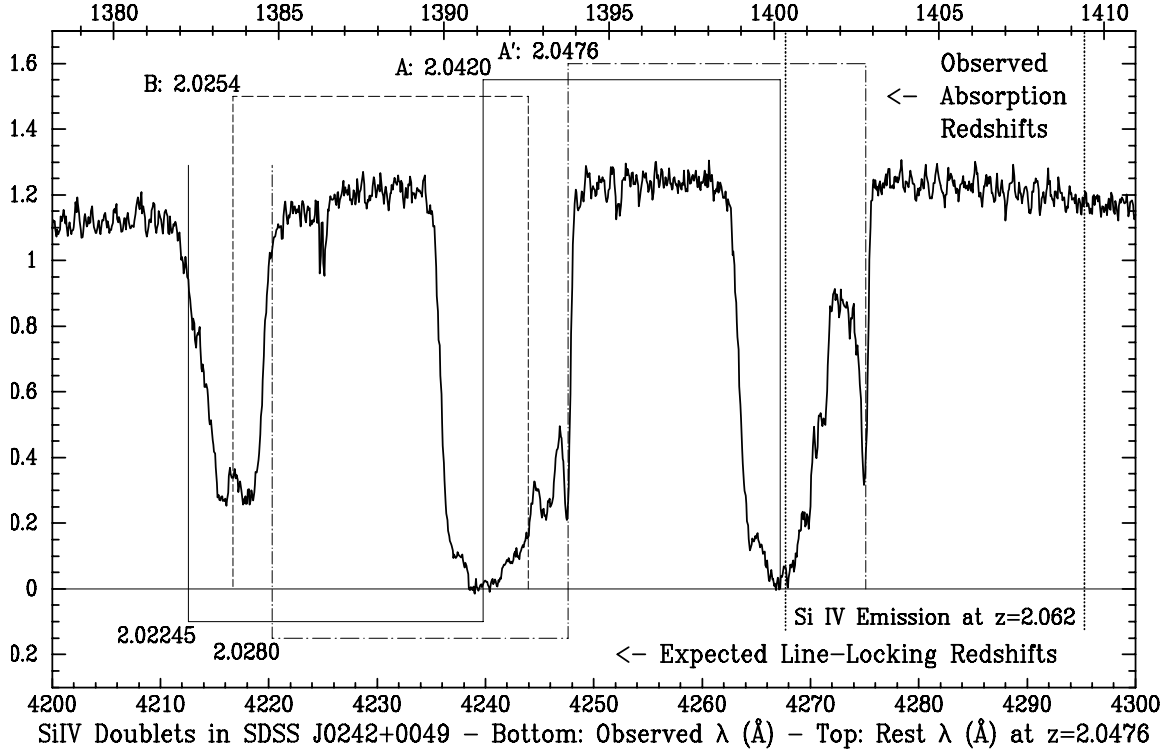
FIG. 4.— Two broad, overlapping Si IV doublets in the unnormalized spectrum of SDSS J0242+0049. Line identifications and redshifts for the different troughs are given on the figure. There is also narrow Si IV absorption at z=2.0314 which is not marked.
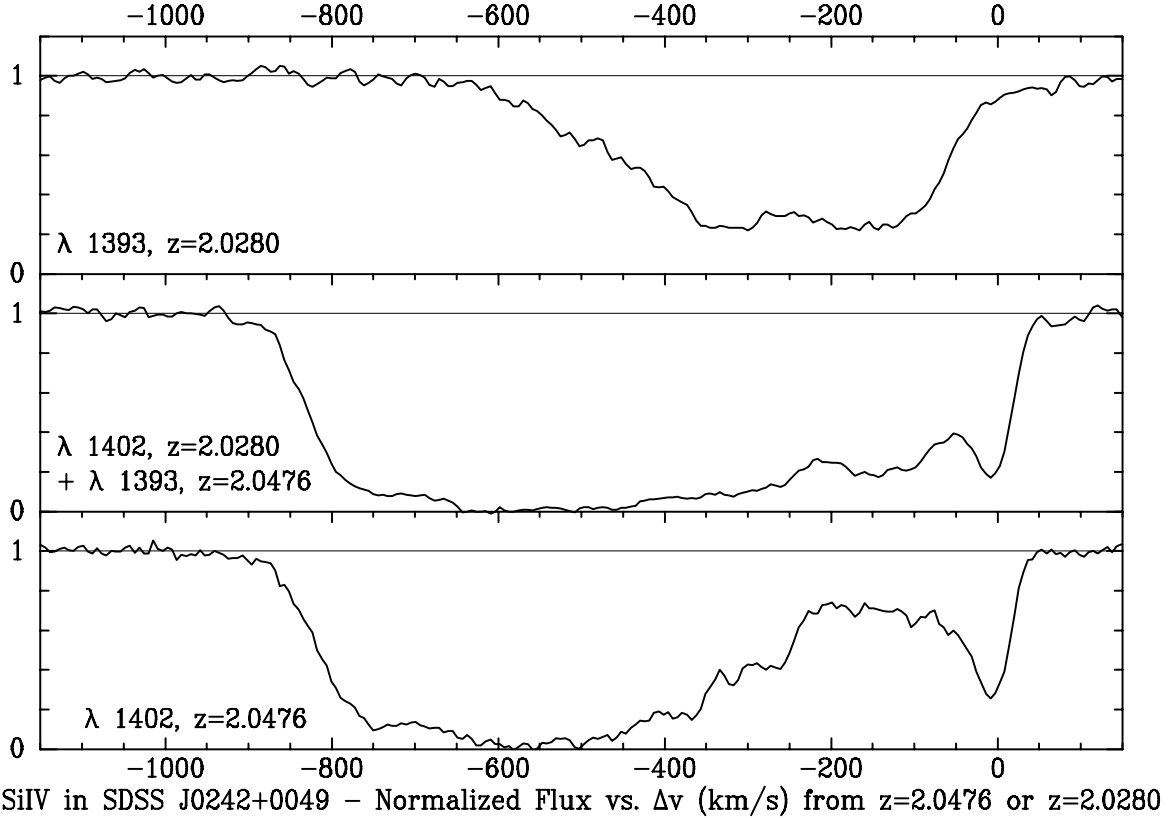

FIG. 5.— Velocity plot of Si IV absorption after normalization by a fit to the total spectrum (continuum and weak emission lines).
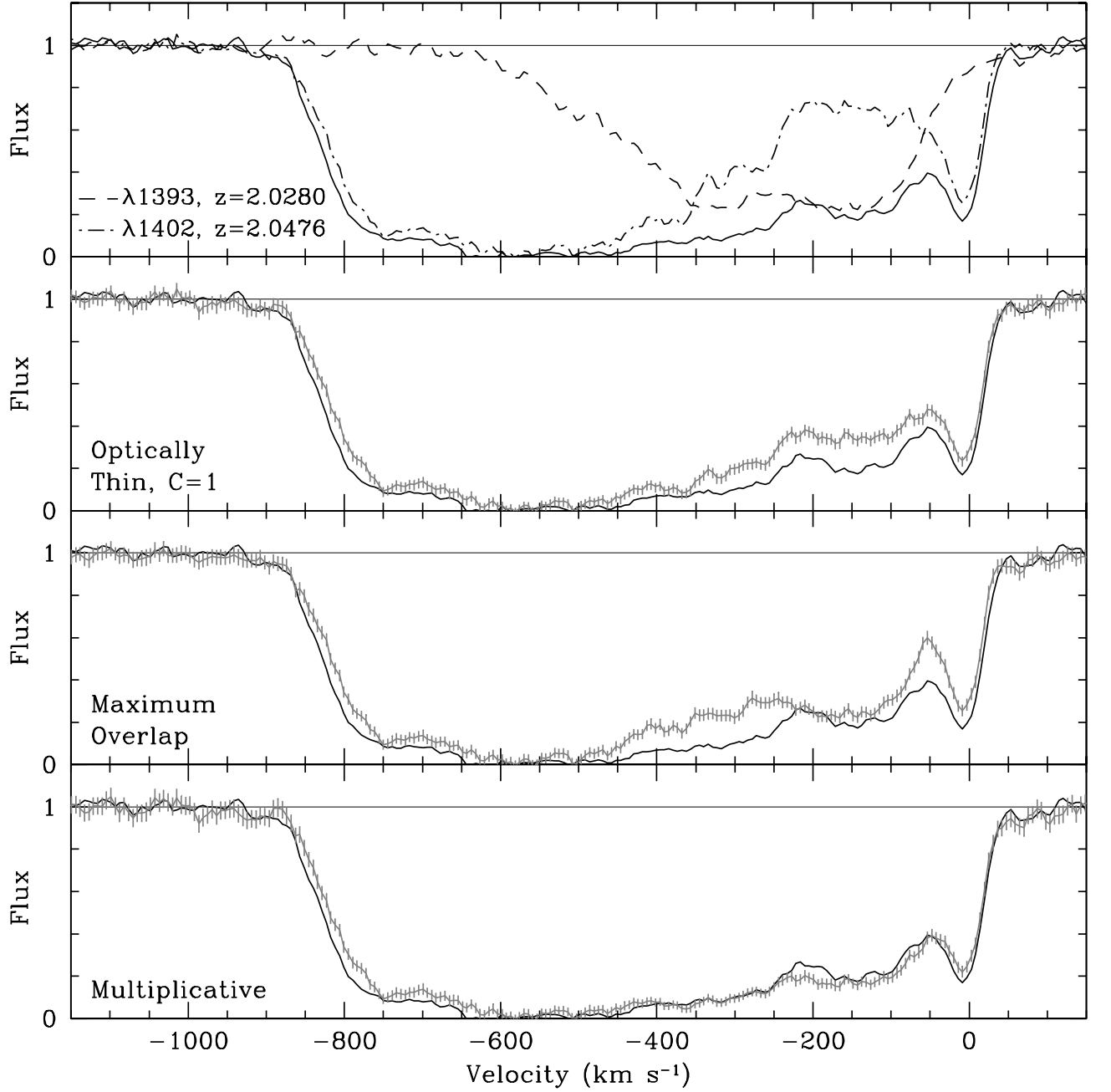
Fig. 6.— Fits to the blended Si IV trough. The trough containing blended absorption from both redshift systems is shown as the solid line in all panels. The fits are shown as lighter lines with *total* error bars that include the observed errors on the flux in the blended trough, so that at each pixel the deviation between the actual trough and the fit can be directly compared to the total accompanying uncertainty. **Top panel:** all three observed Si IV troughs are overplotted. The dashed line shows the unblended trough $\lambda1393$ trough, plotted in the $z = 2.0280$ frame. The dot-dashed line shows the unblended trough $\lambda1402$ trough, plotted in the $z = 2.0476$ frame. **Second panel:** the fit and errors shown are for an optically thin lower-redshift system. **Third panel:** the fit and errors shown are for an optically thick lower-redshift system with maximum overlap in covering factor with the optically thick higher-redshift system. **Bottom panel:** the fit and errors shown are for the case where each system's covering fraction describes its fractional coverage of the other absorption system, so that the residual flux from both optically thick troughs can be multiplied together to give the residual flux in this blended trough.
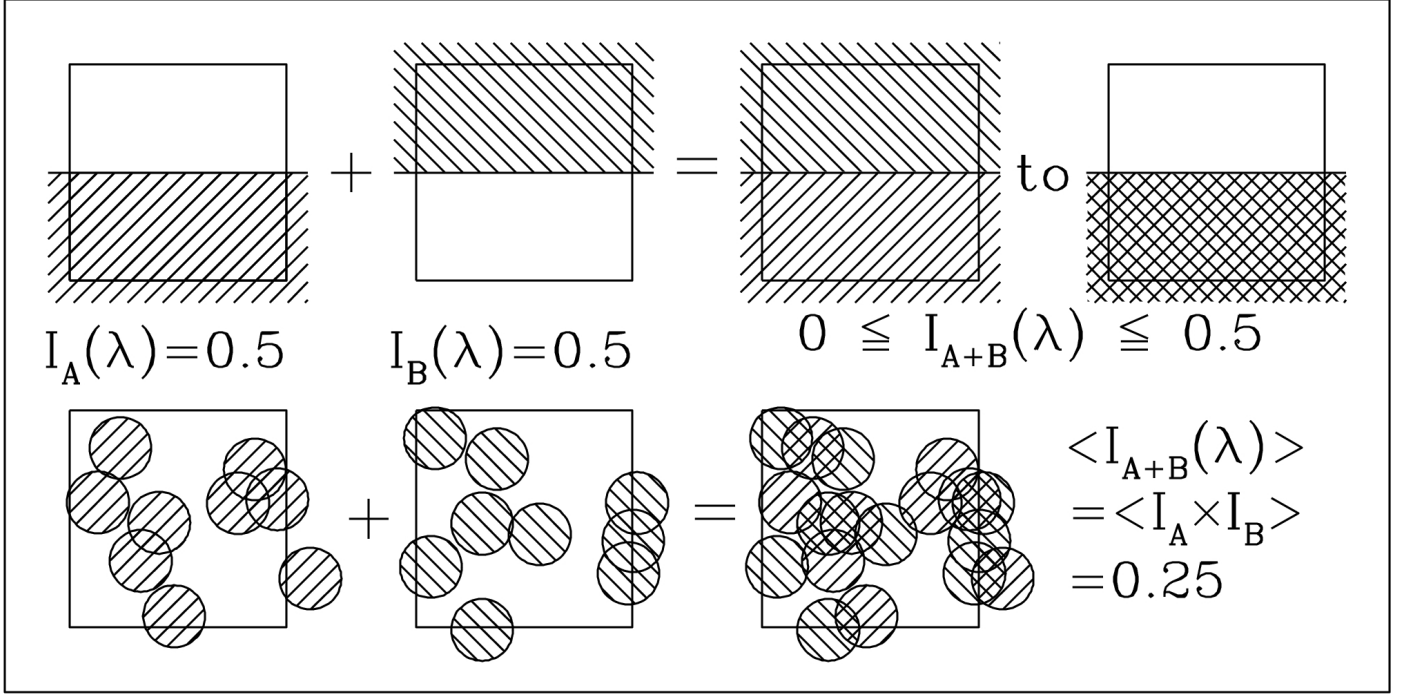
Fig. 7.— An illustration of how observations of optically thick absorption systems overlapping in velocity space can constrain absorber substructure. Each square is a schematic depiction of a quasar's emission region at the same wavelength λ. The hatched zones are the areas of the emission region covered by an absorber. The leftmost column depicts absorption by system A only, which is assumed to produce a normalized residual intensity of $I_A(\lambda) = 0.5$ at the wavelength shown. The value of $I_A(\lambda)$ is the same regardless of whether the absorption is due to a monolithic flow (top row) or due to randomly placed subunits (bottom row), here shown as spheres in projection. Similarly, the second column from the left depicts absorption by system B only, which is also assumed to produce a normalized residual intensity of $I_B(\lambda) = 0.5$ at the wavelength shown. When systems A and B overlap, monolithic flows can produce any normalized residual intensity in the range $0 \leq I_{A+B}(\lambda) \leq 0.5$ (top row, right) depending on the specific areas covered by each flow at that wavelength λ. On the other hand, flows consisting of many randomly placed subunits will naturally yield an average value of $<I_{A+B}(\lambda)>=<I_A(\lambda) \times I_B(\lambda)>= 0.25$ *at every wavelength λ where the systems overlap* (bottom row, right). Deviations from this average will occur due to statistical fluctuations, which will be smaller the more subunits there are. Measuring the deviations thus enables us to constrain the size and number of the subunits (see §4.1.1).